Supplemental Material for

Implementation of cell-free biological networks at steady state

Henrike Niederholtmeyer, Viktoria Stepanova, and Sebastian J. Maerkl

This file includes:

Supplementary Figures S1-S18

Supplementary Tables S1-S2

Supplementary text

References (*1-11*)

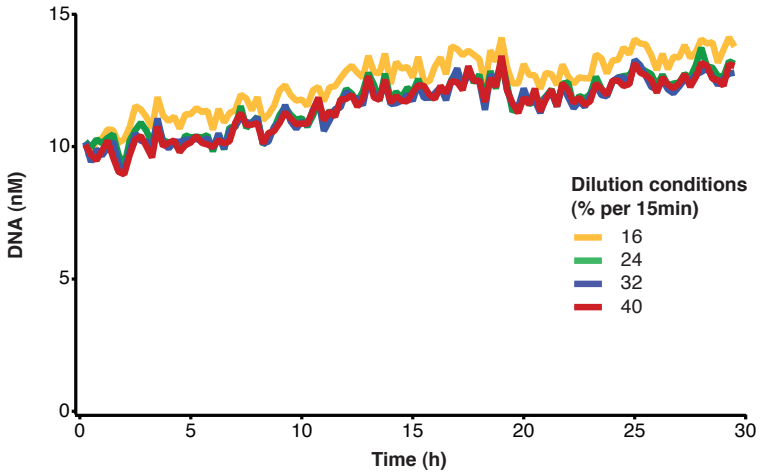

Fig. S1. DNA concentration during steady state ITT. DNA concentration during the steady state reaction at different dilution rates shown in Fig. 2B was monitored via Cy5 fluorescence of the labeled DNA template.

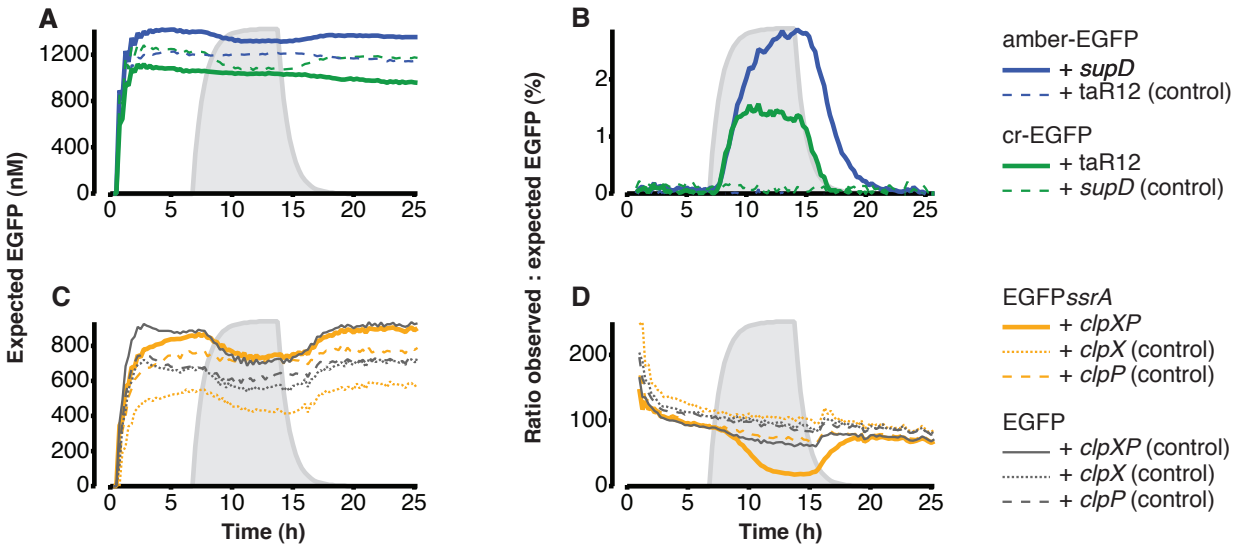

Fig. S2. Quantitative effects of post-transcriptional regulators. (**A**) Expected EGFP concentration calculated from measured mRNA concentrations for translational activation (Fig. 3C). (**B**) Ratio of observed to expected EGFP concentration, translation efficiency. (**C**) Expected EGFP concentration calculated from measured mRNA concentrations for protein degradation (Fig. 3D). (**D**) Ratio of observed to expected EGFP concentration to quantify the influence of protein degradation.

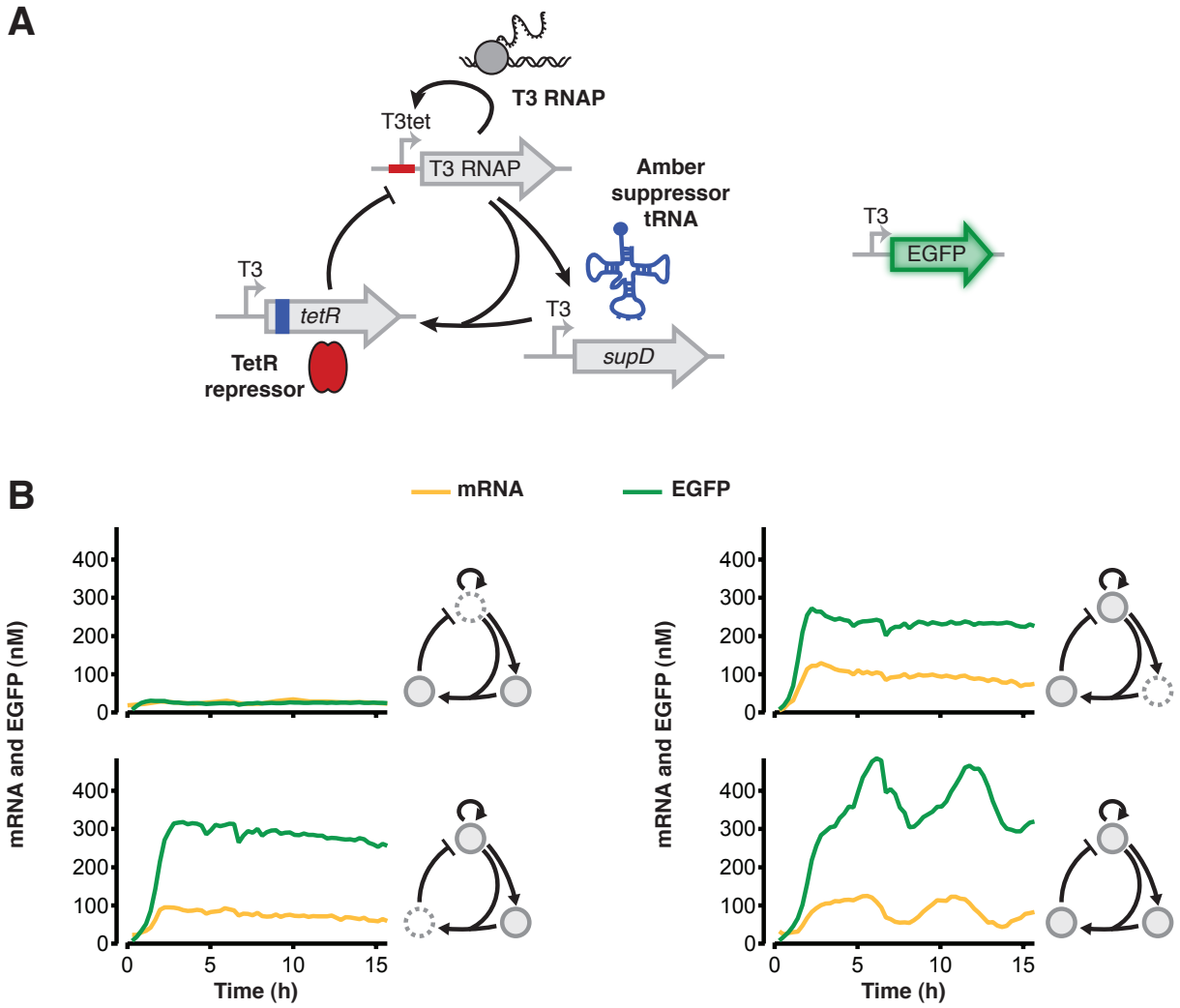

Fig. S3. Influence of the three oscillator genes. (**A**) Network design of the genetic oscillator. The TetR operator in the T3tet promoter and the amber stop codon in the *tetR* gene are indicated as red and blue boxes respectively. Concentrations of the oscillator DNA templates were 5nM T3tet-T3RNAP, 60nM T3-supD, 10nM T3-amber-tetR. We used the T3-EGFP reporter (5nM) with probe target site to determine mRNA concentration of the reporter during the reaction. (**B**) One network component was omitted at a time to determine if they were necessary to produce oscillations. Reactions were performed with a residence time of 49 min.

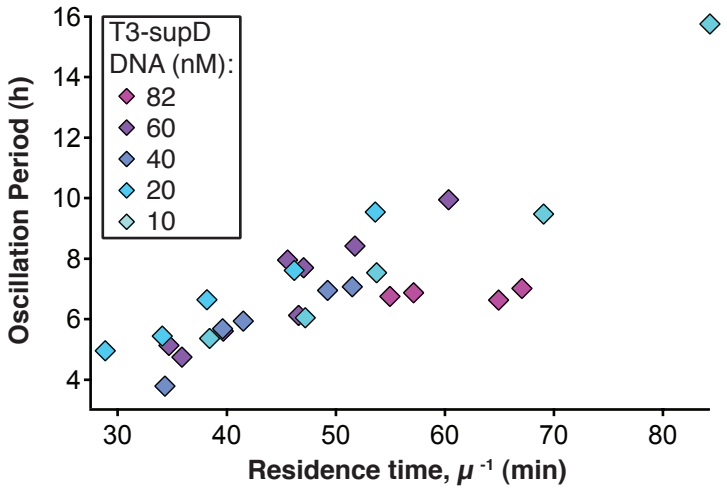

Fig. S4. Oscillation period versus residence time. Oscillation periods from experiments with different T3-*supD* DNA concentration (Figure 4) were plotted against residence time.

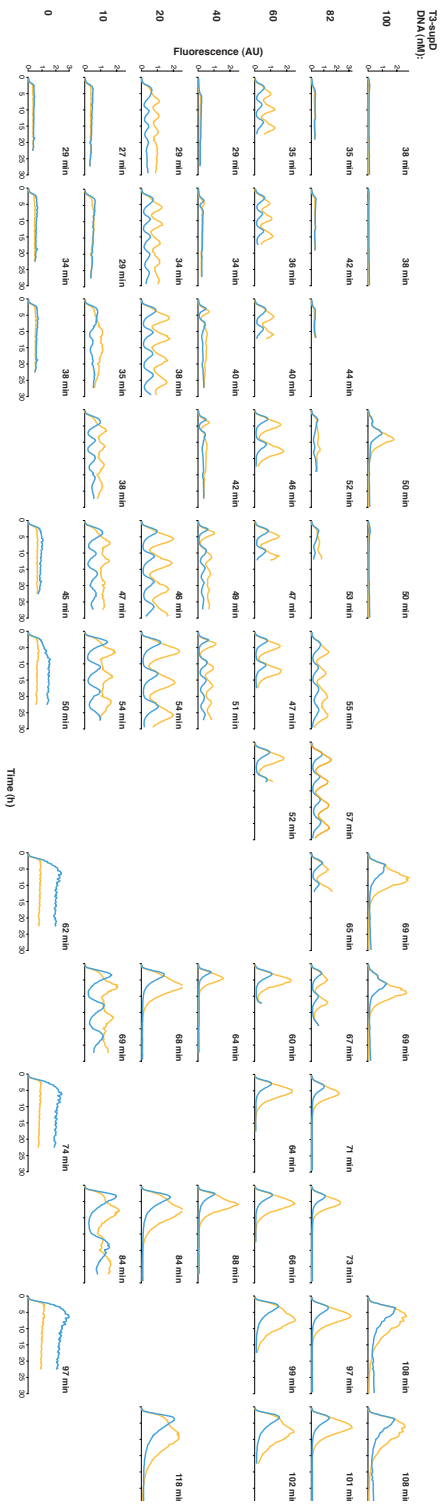

Fig. S5. Results of all oscillator experiments shown in Figure 4B. The graphs are ordered as in the phase diagram (Figure 4B) by T3-*supD* DNA concentration and residence time, which is noted for each graph in the top right.

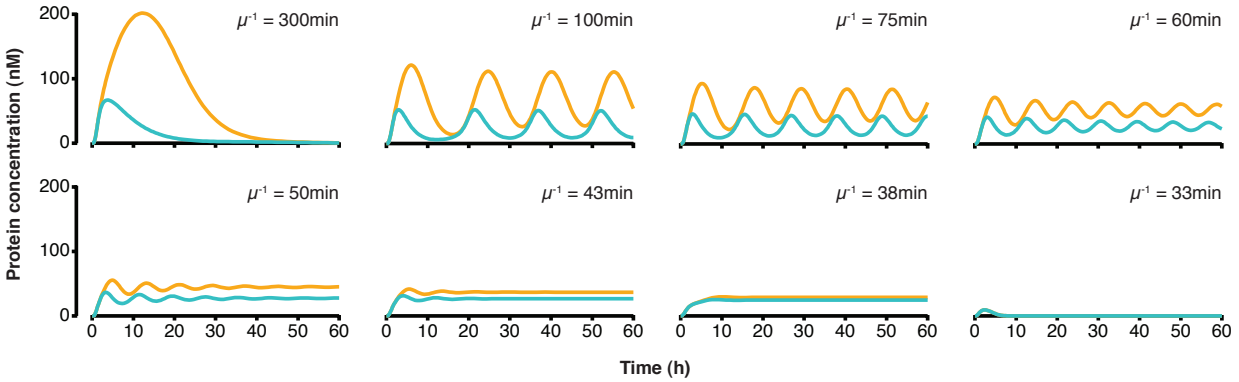

Fig. S6. Influence of dilution rate on oscillatory behavior of the model. Dilution rate, dil (μ), was varied in the model of the genetic oscillator (see SI text and Fig. 4A). Here, we show the concentrations of fluorescent Citrine (yellow lines) and fluorescent Cerulean (blue lines). For comparison to experimental results see Fig. 4 and Fig. S5.

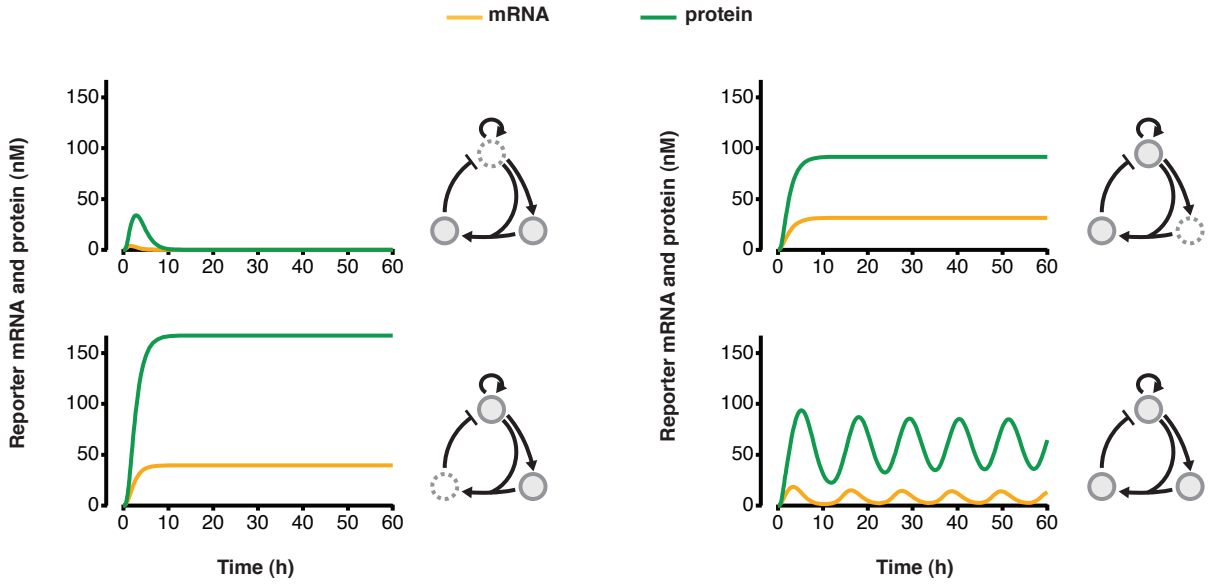

Fig. S7. Influence of the three oscillator genes in the model. The transcription rate of one oscillator gene at a time was set to 0 (top left $TXmax_{T3RNAP} = 0$, top right $TXmax_{supD} = 0$, bottom left $TXmax_{tetR} = 0$, bottom right all TXmax at default value). Reporter mRNA and protein of Citrine under control of the T3 promoter are shown. Dilution rate, dil, was set to $0.8h^{-1}$, which corresponds to a residence time of 75min. For comparison to experimental results see Fig. S3.

Table S1. Oligonucleotide primers used in the study.

Use and primer name	Sequence
Gene specific primers	
Color annotations: Ribosomal binding site Amber stop codon ssrA tag	
EGFP/Citrine-fwd	CCTCTAGAAATAATTTTGTTTAACTTAAGAAGGAGGAAAAAAAAATGTCTA AAGGTGAAGAATTATTCAC
amber-EGFP-fwd	CCTCTAGAAATAATTTTGTTTAACTTAAGAAGGAGGAAAAAAAAATGTAGA AAGGTGAAGAATTATTCACTG
EGFP/Citrine-rev	GTAGCAGCCTGAGTCGTTATTATTTGTACAATTCATCCATACCATGG
EGFP-ssrA-rev	GTAGCAGCCTGAGTCGTTATTAAGCAGCCAGAGCGTAGTTTTCGTCGTTAG CAGCTTTGTACAATTCATCCATACCATGG
T3RNAP-fwd	CCTCTAGAAATAATTTTGTTTAACTTAAGAAGGAGGAAAAAAAA ATGAACATCATCGAAAACATCG
T3RNAP-rev	GTAGCAGCCTGAGTCGTTA TTATGCAAAGGCAAAGTCAGAC
rpoD-fwd	CCTCTAGAAATAATTTTGTTTAACTTAAGAAGGAGGAAAAAAAA ATGGAGCAAAACCCGCAG
rpoD-rev	GTAGCAGCCTGAGTCGTTATTATTAATCGTCCAGGAAGCTACGC
tetR-fwd	CCTCTAGAAATAATTTTGTTTAACTTAAGAAGGAGGAAAAAAAAATGTCCA GATTAGATAAAAGTAAAG
amber-tetR-fwd	CCTCTAGAAATAATTTTGTTTAACTTAAGAAGGAGGAAAAAAAAATGTAGA GATTAGATAAAAGTAAAG
tetR-rev	GTAGCAGCCTGAGTCGTTATTAAGACCCACTTTCACATTTAAG
clpX-fwd	CCTCTAGAAATAATTTTGTTTAACTTAAGAAGGAGGAAAAAAAAATGACA GATAAACGCAAAGATG
clpX-rev	GTAGCAGCCTGAGTCGTTATTA TTCACCAGATGCCTGTTG
clpP-fwd	CCTCTAGAAATAATTTTGTTTAACTTAAGAAGGAGGAAAAAAAAATGTCAT ACAGCGGCGAAC
clpP-rev	GTAGCAGCCTGAGTCGTTATTAATTACGATGGGTCAGAATCGAATC
Cerulean-fwd	CCTCTAGAAATAATTTTGTTTAACTTAAGAAGGAGGAAAAAAAAATGAGTA AAGGAGAAGAACTTTTC
Cerulean-rev	GTAGCAGCCTGAGTCGTTATTATTTGTATAGTTCATCCATGCC
5' extension primers:	
Color annotations: Promoter tet operator	
5'ext-T7	GATCTTAAGGCTAGAGTACTAATACGACTCACTATAGGGAGACCACAACG GTTTCCCTCTAGAAATAATTTTGTTTAAC
5'ext-T7tet	GATCTTAAGGCTAGAGTACTAATACGACTCACTATAGGGAGATCTCCCTAT CAGTGATAGACCTCTAGAAATAATTTTGTTTAAC
5'ext-T3	GATCTTAAGGCTAGAGTACAATTAACACTCACTAAAGGGAGACCTCTAGAA ATAATTTTGTTTAAC

5'ext-T3tet	GATCTTAAGGCTAGAGTACTCCCTATCAGTGATAGAATTAACACTCACTAA AGGGAGATCCCTATCAGTGATAGACCTCTAGAAATAATTTTGTTTAAC
5'ext-σ^{70} lac	GATCTTAAGGCTAGAGTACAATTGTGAGCGGATAACAATTGACATTGTGAG CGGATAACAATATAATATGCGCATCCTCTAGAAATAATTTTGTTTAAC
5'ext-σ^{70} tet	GATCTTAAGGCTAGAGTACTCCCTATCAGTGATAGAGATTGACATCCCTAT CAGTGATAGATATAATATGCGCATCCTCTAGAAATAATTTTGTTTAAC

3' extension primers:
Color annotations: Terminator binary probe target

3'ext_no-tgt	CAAAAAACCCCTCAAGACCCGTTTAGAGGCCCCAAGGGGTTATGCTAGTTT TTTTTTTTTTTTTTTTTTTTTTTTTTGTAGCAGCCTGAGTCG
3'ext_3'tgt-3	CAAAAAACCCCTCAAGACCCGTTTAGAGGCCCCAAGGGGTTATGCTAGTTT TTTTTTTTTTTTTTTTTTTTTTTTTTGATAGAGTCCTTCCACGATACCAATGG GCTCAGTTTTTTGTTTTTTGGGTTTTGGTTTTGTTTTCCAGTACACAGGCGTA GCAGCCTGAGTCG

Final amplification primers:

5'final	GATCTTAAGGCTAGAGTAC or /Cy5/GATCTTAAGGCTAGAGTAC
3'final	CAAAAAACCCCTCAAGAC or /Cy5/CAAAAAACCCCTCAAGAC

Specialized primer sets:
Color annotations: Promoter Ribosomal binding site

supD:

T7-supD-fwd	GATCTTAAGGCTAGAGTACTAATACGACTCACTATAGGAGAGATGCCGGA GCGGCTGAACGGACCGGTCTC
T3-supD-fwd	GATCTTAAGGCTAGAGTACAATTAACACTCACTAAAGGAGAGATGCCGGA GCGGCTGAACGGACCGGTCTC
supD-rev	TGGCGGAGAGAGGGGGATTTGAACCCCCGGTAGAGTTGCCCCTACTCCGGT TTTAGAGACCGGTCCGTTCAGCCG

T7-cr-EGFP:

cr-EGFP-fwd (gene specific primer)	GGGTATTAAAGAGGAGAAAGGTACCATGTCTAAAGGTGAAGAATTATTCA C
5'ext-crR12-5' (upstream part of 5'ext)	GATCTTAAGGCTAGAGTACTAATACGACTCACTATAGGGAGAATTCTACCA TTCACC
5'ext-crR12-3' (downstream part of 5'ext)	GGTACCTTTCTCCTCTTTAATACCCAAATCCAAGAGGTGAATGGTAGAATT CTCCCT

T7-taR12:

T7-taR12-fwd	GATCTTAAGGCTAGAGTACTAATACGACTCACTATAGGACCCAAATCCAGG AGGTGATTGGTAG
taR12-rev	TCTAGAGATATATGGTAGTAGTAAGTTAATTTTCATTAACCACCACTACCA ATCACCTCCTGGATTTG

Table S2. DNA template concentrations for experiments in Figure 3. All reporter DNA templates contained a target site for binary probes to determine EGFP mRNA concentrations. DNA constructs are named by promoter name (see Table S1 for sequence) followed by a hyphen and the name of the controlled gene.

Experiment	Regulator DNA	Reporter DNA
Transcriptional activation (Figure 3A)		
by T3 RNA polymerase		
	1nM T7-T3RNAP	5nM T3-EGFP
control	1nM T7-rpoD	5nM T3-EGFP
by sigma factor 70 (σ^{70}, *rpoD*) in combination with *E. coli* RNA polymerase core enzyme		
	1nM T7-rpoD	10nM σ^{70}tet-EGFP
control	1nM T7-T3RNAP	10nM σ^{70}tet-EGFP
Transcriptional repression by TetR (Figure 3B)		
T7 RNA polymerase promoter		
	1nM T7-tetR	4nM T7tet-EGFP
control	1nM T7-tetR	4nM T7-EGFP
T3 RNA polymerase promoter		
	1nM T7-tetR	4nM T3tet-EGFP
control		
	1nM T7-tetR	4nM T3-EGFP
E. coli RNA polymerase σ^{70} promoter		
	1nM T7-tetR	4nM σ^{70}tet-EGFP
control	1nM T7-tetR	4nM σ^{70}lac-EGFP
Translational activation (Figure 3C)		
by amber suppressor tRNA (*supD*)		
	20nM T7-supD	10nM T7-amber-EGFP
control	20nM T7-taR12	10nM T7-amber-EGFP
by trans-activator RNA (taR12)		
	20nM T7-taR12	10nM T7-cr-EGFP
control	20nM T7-supD	10nM T7-cr-EGFP
Protein degradation by ClpXP (Figure 3D)		
of EGFP with degradation tag (ssrA)		
	2nM T7-clpX + 2nM T7-clpP	4nM T7-EGFP-ssrA
control	2nM T7-clpX	4nM T7-EGFP-ssrA
control	2nM T7-clpP	4nM T7-EGFP-ssrA
of EGFP without degradation tag		
control	2nM T7-clpX + 2nM T7-clpP	4nM T7-EGFP
control	2nM T7-clpX	4nM T7-EGFP
control	2nM T7-clpP	4nM T7-EGFP

Design and fabrication of the microfluidic chip

We designed a two-layer microfluidic chip to perform ITT reactions at steady state (Figure S8). The design of the microfluidic chip is similar to previous devices (1-3). One chip contains eight reaction rings to simultaneously run eight independent experiments. Different reagents can be connected to nine fluid inlets, which can be addressed by a multiplexer. Fluid bypasses allow rapid flushing of channels leading to the reaction rings. The inlet of each reaction ring can be opened and closed independently from the others. A peristaltic pump in front of the rings is used to meter reagents into the reaction rings. A second peristaltic pump is used to mix the contents inside the rings. The design allowed us to use different dilution rates or different template DNAs in each of the nanoreactors. Each nanoreactor had a volume of 33nL.

Molds for the control and the flow layer were fabricated on separate wafers by standard photolithography techniques and patterned with photoresist to produce channels with the heights stated in Figure S8. To ensure a homogenous film of photoresist on the mold for the flow layer, we applied the thinner AZ9260 first, and developed, before we spin-coated the thicker SU8 layer. The microfluidic chips were fabricated from PDMS by standard multilayer soft lithography (4). The control layer was located at the bottom of the chip and plasma bonded to a glass slide.

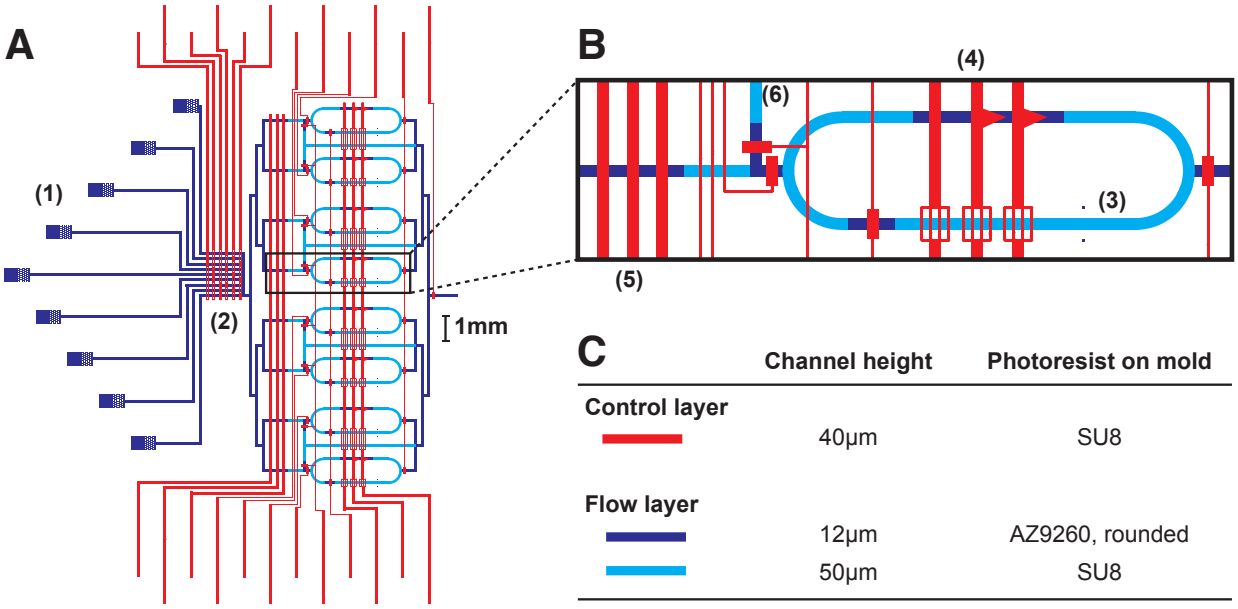

Fig. S8. Design of the microfluidic chip. (**A**) Design of the full microfluidic device. (**B**) Close-up of a reaction ring. The control layer is shown in red and the flow layer in two shades of blue. The width of a flow channel or a control valve is 100µm. (1) Reagent inlets, (2) multiplexer, (3) reaction ring and imaging position, (4) peristaltic pump for mixing of reagents in the reaction ring, (5) peristaltic pump to add reagents into the reaction ring, (6) bypass channel. (**C**) Channel heights and photoresists used.

Operation of the microfluidic chip

Pressure of microfluidic flow and control was regulated by a custom pneumatic setup. Control lines were set to 40psi, except the three lines, which controlled the peristaltic mixing pump, which were set to 20 psi using a separate pressure gauge and were additionally connected to a vacuum pump. Microfluidic valves were actuated by computer-controlled solenoid valves operated by a custom written LabView program. Depending on the experiment, flow pressure was regulated between 5 and 9psi to achieve additions between 0.4 and 1% of the ring volume per pump cycle. Usually, the flow pressure was set to the value where one pump cycle of the peristaltic input pump corresponded to 0.8% of the reactor volume.

The device was placed on an automated microscope in an opaque, temperature controlled incubation chamber, which allowed fluorescent imaging and a constant reaction temperature set to 37°C. One critical feature enabling long-term reaction conditions, was cooling of the ITT mixture before it enters the microfluidic chip, which was accomplished with a combination of a peltier element and water cooled heat sink (Figure S9). The volume of ITT mixture for the entire experiment was aspirated into a FEP (fluorinated ethylene propylene) tube, for storage on the peltier element. This tube was then connected to the microfluidic chip via a PEEK (polyether ether ketone) tube (Vici) with a thin inner diameter (180µm) to reduce the volume of un-cooled ITT reagent. For all other reagents we used tygon tubing without cooling.

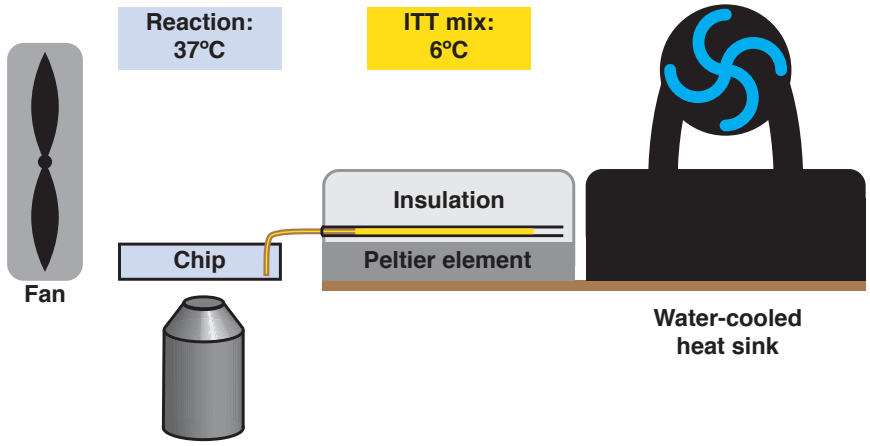

Fig. S9. Cooling of the ITT mix. Schematic of the custom-built cooling system for the ITT mix. The FEP tube holding the ITT mix for the experiment is held on top of a peltier element (Laird Technologies), it is connected to the microfluidic chip via a PEEK tube with a thin inner diameter (180µm). The heat sink for the peltier element is a copper plate cooled by a CPU cooler (EK waterblocks) connected to a water pump regulated to 8°C (Solid State cooling systems). In order to prevent condensation and ice formation on the edge of the peltier element facing the microfluidic chip, we placed a fan on the opposite site of the device. This temperature control system kept the ITT mix in the storage tube at approximately 6°C while the on-chip reaction temperature was 37°C, the temperature in the incubation chamber enclosing the setup.

Characterization of the microfluidic chip

The volume added into the reaction rings per pump cycle of the peristaltic input pump was consistent across the eight reactors on the chip and increased linearly with the number of pump cycles (Figure S10A). Before each experiment, the dilution rate was determined by measuring the washout rate of EGFP fluorescence (Figure S10B).

We measured the speed at which reagents inside the reaction rings were mixed by adding a plug of fluorescent EGFP solution into the rings. One position of the channel was imaged while the peristaltic pump started moving the fluorescent plug in a circle leading to mixing (Figure S11). Within less than 2 min mixing was completed.

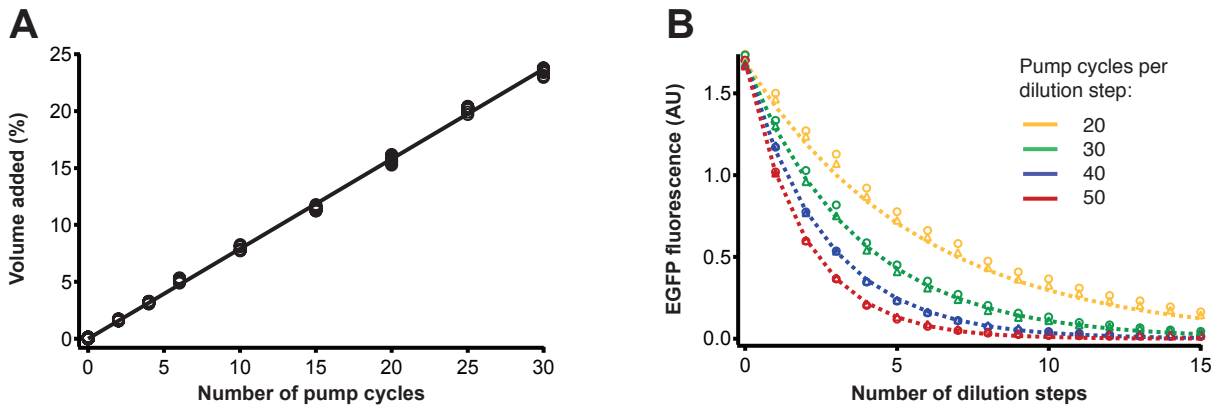

Fig. S10. Characterization of the peristaltic input pump. (**A**) Volume added into the reactors depends linearly on the number of pump cycles. Shown are the results from eight reactors of the same device. (**B**) Washout from the reactor at different dilution rates. Shown are the results of eight reactors from one device, with two repeats of each dilution rate (markers), and the prediction for a washout of 16, 24, 32 and 40% of reactor volume per dilution step (dashed lines). In both panels one pump cycle displaced 0.8% of the reactor volume.

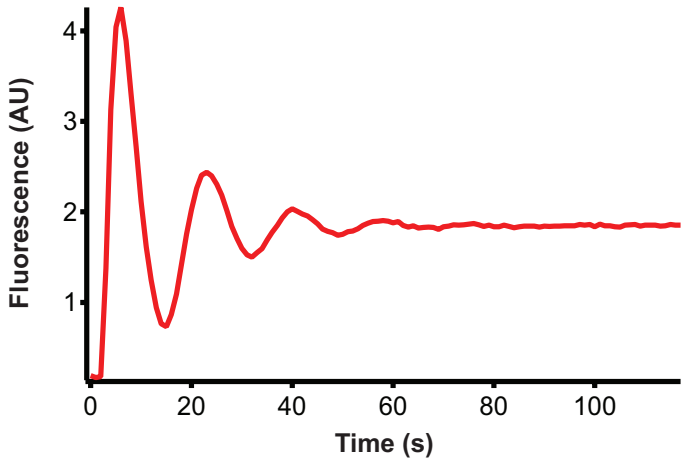

Fig. S11. Mixing of reagents in the reaction rings. To reaction rings filled with 2% BSA in PBS a plug of 7% of the reactor volume of 100µg/ml EGFP was added with the peristaltic input pump. The reactor channel was imaged while the peristaltic mixing pump moved the EGFP plug in a circle, causing the solutions to mix.

Experimental procedure

Priming and calibration
At the beginning of each experiment the device was primed with a solution of 2% BSA in PBS. Then, the dilution rates were calibrated as shown in Fig. S10B. This ensured correct functioning of the device before start of the experiment and to adjust the dilution rates to the desired value.

Steady state ITT reaction
Operation of the microfluidic chip and imaging during steady state ITT reactions was fully automated with a custom written LabView program. The sequence of operations was as follows:

Step	Operation
0	Initial fill: - flush reactors with ITT mixture - meter 20% reactor volume of template DNA into the reactors - mix
	Repeat the following steps every 15min:
1	Image each reactor
2	Flush the bypass channels with buffer
3	Addition of fresh ITT mix: - flush the bypasses channels with ITT mixture - add 4*n pump cycles of ITT mixture into the reactors - flush the bypass channels with buffer
4	Addition of DNA: - flush the bypasses channels with DNA solution - add n pump cycles of DNA into the reactors - flush the bypass channels with buffer
5	Mix
6	Repeat from step 1

Flushing of the bypass channels with costly reagents like ITT mixture and DNA solutions was done with the peristaltic input pump in order to reduce reagent consumption. For a complete experiment of 30h, only 6.25µl of ITT mixture were required per reactor. The buffer used for flushing was 5mM Tris-HCl pH8.5. The peristaltic mixing pump was actuated with a frequency of 8.3Hz. The input pump was actuated with a frequency of 1.7Hz for flushing the bypass channel, and with a frequency of 0.3Hz to add reagents into the reactions rings.

Rate measurements and model

Model of a batch ITT reaction

We describe the ITT reaction in batch with a set of six differential equations

DNA, *d*:
[1] $d'(t) = 0$

mRNA, *m*:
[2] $m'(t) = TX(d) \cdot act_{TX}(t) - \deg_m \cdot m(t)$

dark (immature) EGFP, p_d:
[3] $p_d'(t) = TL(m) \cdot act_{TL}(t) - mat \cdot p_d(t)$

fluorescent (mature) EGFP, p_f:
[4] $p_f'(t) = mat \cdot p_d(t)$

Relative transcriptional activity, act_{TX}:
[5] $act_{TX}'(t) = -\deg_{TX} \cdot act_{TX}(t)$

Relative translational activity, act_{TL}:
[6] $act_{TL}'(t) = -\deg_{TL} \cdot act_{TL}(t)$

We determined each parameter of this model in separate experiments. TX is the initial transcription rate that depends on DNA template concentration. TL is the initial translation rate that depends on mRNA concentration. We assume an unspecific decrease of those activities as a function of time and use act_{TX} and act_{TL} as the relative activities left at a given time. RNA, transcriptional activity and translational activity degrade/decrease with rates deg_m, deg_{TX}, deg_{TL} respectively. Dark EGFP matures to fluorescent EGFP with the rate *mat*. We did not observe any degradation of fluorescent EGFP.

Degradation of mRNA

The rate of mRNA degradation was determined as in (5) by monitoring the decrease of a known concentration of purified mRNA,m_0, in an on-chip batch reaction (Figure S12). The decreasing RNA concentration was fit to the solution of equation [2], with TX=0:

[7] $m(t) = m_0 \cdot e^{-\deg_m \cdot t}$

In different experiments and at different initial RNA concentrations we measured degradation rates between 0.003 and 0.008 min^{-1}. For the model, we used a RNA degradation rate deg_m of 0.003 min^{-1}.

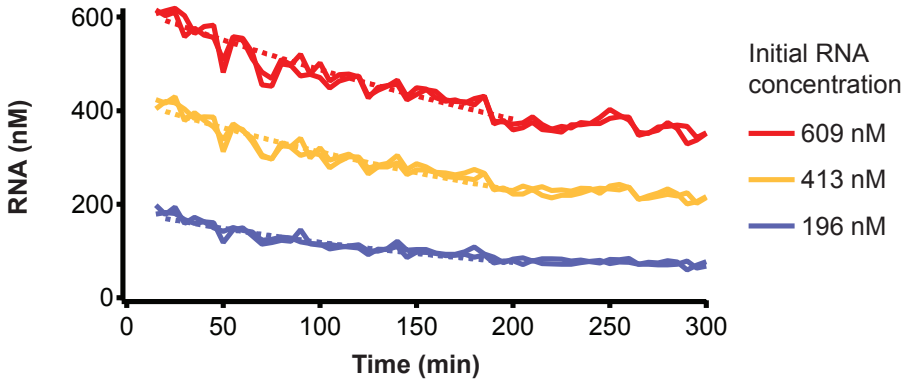

Fig. S12. Measurement of mRNA degradation rate. Different concentrations of purified mRNA were added to an ITT reaction on chip. Concentration of mRNA was monitored over time and fit to equation [7] (dashed lines).

Initial rate of transcription

We determined the initial transcription rate as a function of DNA in an on-chip batch reaction as in (5). The initial change in mRNA concentration can be described by equation [8] and we fit RNA concentration during the initial phase of the reaction to the solution, equation [9] (Figure S13A).

[8] $m'(t) = TX(d) - \deg_m \cdot m(t)$

[9] $m(t) = \frac{TX(d)}{\deg_m} \cdot (1 - e^{-\deg_m \cdot t})$

Transcription can be described by Michaelis-Menten kinetics:

[10] $TX(d) = \frac{TX_{\max} \cdot d}{K_{TX} + d}$

The maximal initial transcription rate, TX_{max}, was 11.5 nM/min and the DNA concentration for half maximal activity, K_{TX}, was 5.5nM (Figure S13B).

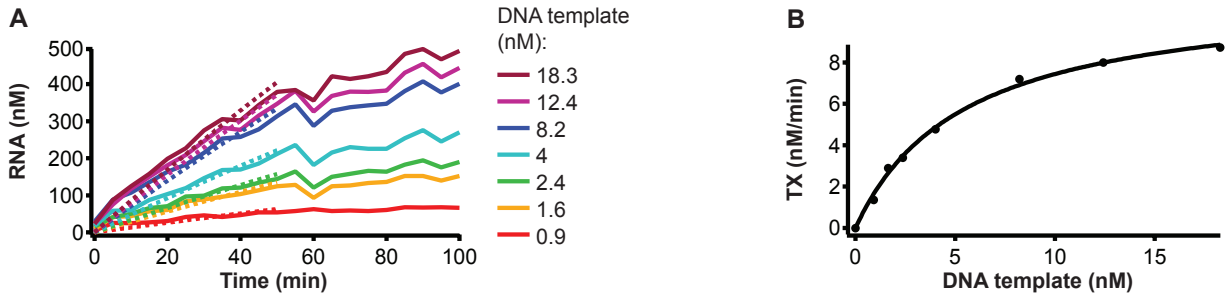

Fig. S13. Measurement of initial transcription rate. (**A**) RNA synthesis from different DNA template concentrations was monitored and the concentration during the initial 50 min of the reaction was fit to equation [9] using a fixed mRNA degradation rate, deg_m, of 0.003 min^{-1} (dashed lines) to determine TX(d). (**B**) Initial transcription rates as determined in (A) and fit to Michaelis-Menten kinetics (equation [10]).

Relative transcriptional activity over time

The relative transcriptional activity of an on-chip batch reaction over time was determined for RNA synthesis from different template DNA concentrations as in (5) using Euler's method (Figure S14):

[11] $m(t+\Delta t) = m(t) + (TX(d) \cdot act_{TX}(t) - \deg_m \cdot m(t)) \cdot \Delta t$

[12] $act_{TX}(t) = \dfrac{m(t+\Delta t) - m(t) + \deg_m \cdot m(t) \cdot \Delta t}{TX(d) \cdot \Delta t}$.

We approximated the mode of transcriptional activity decrease by exponential decay (see equation [5]). The rate of the decrease in relative transcriptional activity, $\deg_{TX}$, was on average 0.005 min^{-1}.

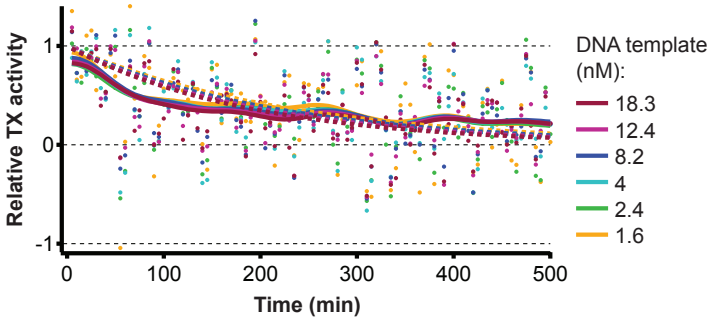

Fig. S14. Relative transcriptional activity over time. The relative transcriptional activity with respect to its initial value was calculated for RNA synthesis from different DNA template concentrations using equation [12] (dots) and the previously determined rates. These traces were smoothed for visualization (lines) and fit to an exponential decay function to determine the rate of decrease (dashed lines).

Maturation of EGFP

To determine the maturation rate of EGFP in our experimental conditions an ITT reaction producing EGFP was stopped by adding RNase, which immediately stops translation. Any increase of EGFP after this addition was therefore due to maturation of dark EGFP to fluorescent EGFP. This simplifies equation [3] to

[13] $p_d'(t) = -mat \cdot p_d(t)$

With this, the solution of equation (4) is:

[14] $p_f(t) = p_0 + \Delta p \cdot (1 - e^{-mat \cdot t})$

p_0 is the concentration of fluorescent EGFP when translation is stopped and Δp is the increase in its concentration when all dark EGFP is completely converted to fluorescent EGFP. EGFP maturation rate was determined to be 0.1 min^{-1} (Fig. S15).

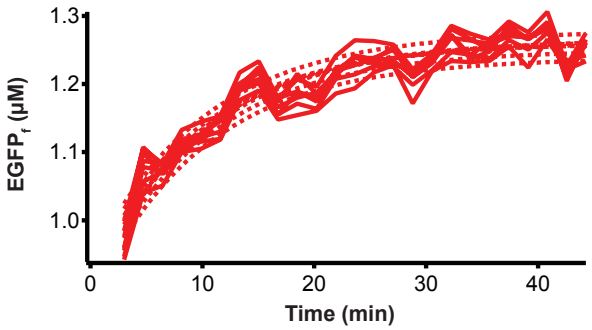

Fig. S15. Maturation of EGFP. After 25 min of an on-chip ITT reaction from a DNA template, translation was stopped by adding 0.6μM RNase. Concentration of fluorescent EGFP after RNase addition (lines) was fit to equation [14] to determine the maturation rate.

Initial rate of translation

We measured EGFP synthesis from different concentrations of purified mRNA. In the initial phase of this reaction, not taking into account a decrease of translational activity over time, this simplifies equations [2] and [3] to

[15] $m'(t) = -\deg_m \cdot m(t)$

[16] $p_d'(t) = TL(m) - mat \cdot p_d(t)$

With $TL(m) = \alpha_{TL} \cdot m(t)$ and $p_f(0)=p_d(0)=0$, the solution of equations [15], [16] and [4]:

[17] $p_f(t) = \frac{\alpha_{TL} \cdot m_0}{\deg_m \cdot (\deg_m - mat)} \cdot (mat \cdot (e^{-\deg_m \cdot t} - 1) + \deg_m \cdot (1 - e^{-mat \cdot t}))$.

Concentration of fluorescent EGFP of the initial phase of the reaction was fit to equation [17] to determine α_{TL} (Fig. S16A). Translation follows Michaelis-Menten kinetics:

[18] $TL(m) = \frac{TL_{max} \cdot m}{K_{TL} + m}$.

K_{TL}, the mRNA concentration at half-maximal translation rate, was determined from multiple benchtop experiments to be 150.2 nM. This K_{TL} was used to determine the average TL_{max} of two independent on-chip reactions. The TL_{max} on-chip was lower than in a benchtop reaction and also more variable (Fig S16B). For the model we used an average value of 76.4 nM/min.

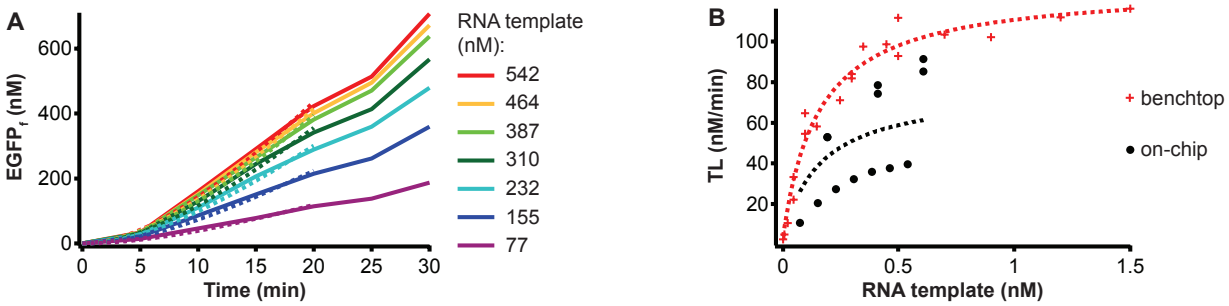

Fig. S16. Measurement of initial translation rate. (**A**) On-chip EGFP synthesis from different mRNA template concentrations was monitored and the concentration during the initial 20 min of the reaction was fit to equation [17] using the known initial mRNA concentration m_0 and the previously determined rates, $\deg_m$ and *mat* (dashed lines) to determine α_{TL}. (**B**) Initial transcription rates, TL, in a benchtop reaction (red crosses) and in two independent on-chip experiments (black circles) as determined in (A) were fit to Michaelis-Menten kinetics (equation [18]) (dashed lines).

Translational activity over time

Translational activity over time was determined by Euler's method. Equations [15], [3] and [4] can be written as

[19] $m(t+\Delta t) = m(t) - \deg_m \cdot m(t) \cdot \Delta t$

[20] $p_d(t+\Delta t) = p_d(t) + \Delta t \cdot (act_{TL}(t) \cdot TL(m) - mat \cdot p_d(t))$

[21] $p_f(t+\Delta t) = p_f(t) + \Delta t \cdot mat \cdot p_d(t)$.

From the known initial mRNA concentration, we calculated the mRNA concentration at each later time point. We had measured the concentration of fluorescent EGFP, p_f. Using smoothed p_f values we determined the concentration of dark EGFP, from equation [21]:

[22] $p_d(t) = \dfrac{p_f(t+\Delta t) - p_f(t)}{\Delta t \cdot mat}$.

This allowed us to calculate the relative translational activity, act_{TL} at each time point, which is the fraction of the initial activity left.

[23] $act_{TL}(t) = \dfrac{p_d(t+\Delta t) - p_d(t) + mat \cdot p_d(t) \cdot \Delta t}{\Delta t \cdot TL(m)}$.

Within one experiment the rate of decrease of translational activity was very consistent and did not depend on the mRNA concentration used (Fig. S17). The average rate of activity decrease determined from two independent on-chip experiments was 0.017min^{-1}.

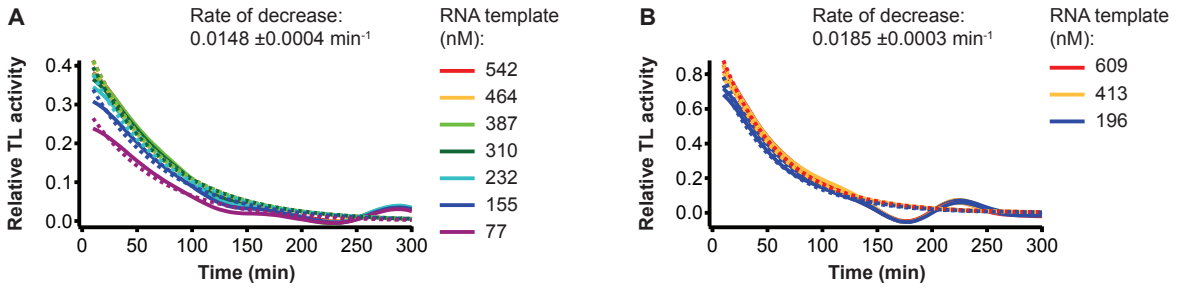

Fig. S17. Relative translational activity over time. In two independent on-chip experiments (**A** and **B**) EGFP was synthesized from different initial concentrations of purified mRNA. The relative translational activity with respect to its initial value was calculated using equations [19], [22], [23] and smoothed $EGFP_f$ measurement traces. The relative activities over time were then fit to an exponential decay function to determine the rate of decrease (dashed lines).

Summary of rates

The rates we measured here for a batch reaction on chip compared well with rates that were previously determined for the same ITT reaction mixture for bench-top reaction with larger volumes (5, 6). The following table summarizes all the rates we determined in the sections above that describe a batch reaction on chip, and that we used in our model:

Rate	**Value**
RNA degradation rate, deg_m	0.003 min^{-1}
Initial transcription rate, TX(d)	$TX(d)\frac{11.5\frac{nM}{\min}\cdot d}{5.5nM + d}$
Rate of relative transcriptional activity decrease, deg_{TX}	0.005 min^{-1}
EGFP maturation rate, *mat*	0.1 min^{-1}
Initial translation rate, TL(m)	$TL(m)\frac{76.4\frac{nM}{\min}\cdot m}{150.2nM + m}$
Rate of relative translational activity decrease, deg_{TX}	0.017 min^{-1}

Model of a continuous reaction with dilutions

To describe the continuous reaction in the microfluidic reactor we modeled the processes of the batch ITT reaction in discrete time intervals, Δt, of one minute. Every 15min a dilution fraction, *dil* (between 0.16 and 0.4, depending on the dilution conditions), was removed from the concentrations of the modeled molecules and the transcription and translation activities, which constitutes the washout. Also every 15min, full transcription and translation activities and DNA concentration, all scaled by fraction *dil*, were added:

		Every 15 min
DNA	$d(t+\Delta t) = d(t)$	$-dil \cdot d(t) + c \cdot dil \cdot d(t)$
mRNA	$m(t+\Delta t) = m(t) + \Delta t \cdot (TX(d) \cdot act_{TX}(t) - \deg_m \cdot m(t))$	$-dil \cdot m(t)$
EGFPd	$p_d(t+\Delta t) = p_d(t) + \Delta t \cdot (TL(m) \cdot act_{TL}(t) - mat \cdot p_d(t))$	$-dil \cdot p_d(t)$
EGFPf	$p_f(t+\Delta t) = p_f(t) + \Delta t \cdot mat \cdot p_d(t)$	$-dil \cdot p_f(t)$
Rel. TX act	$act_{TX}(t+\Delta t) = act_{TX}(t) - \Delta t \cdot \deg_{TX} \cdot act_{TX}(t)$	$-dil \cdot act_{TX}(t) + dil$
Rel. TL act	$act_{TL}(t+\Delta t) = act_{TL}(t) - \Delta t \cdot \deg_{TL} \cdot act_{TL}(t)$	$-dil \cdot act_{TL}(t) + dil$

Concentration, c, of DNA is usually equal to the initial DNA concentration d(0), in which case DNA concentration is constant. In special cases c can change transiently during the experiment, which leads to a new steady state DNA concentration, c.

Initial conditions

d(0) varied from experiment to experiment. In continuous ITT reactions $m(0)=p_d(0)=p_f(0)=0$ and $act_{TX}(0)=act_{TL}(0)=1$.

Prediction of transcriptional and translational activities at different dilution rates

The predicted relative transcriptional and translational steady state activities depended on the dilution rate. The higher the dilution rate, the higher was the steady state activity. Figure S18 shows the predicted relative transcriptional and translational activities for the experiments of Figure 2.

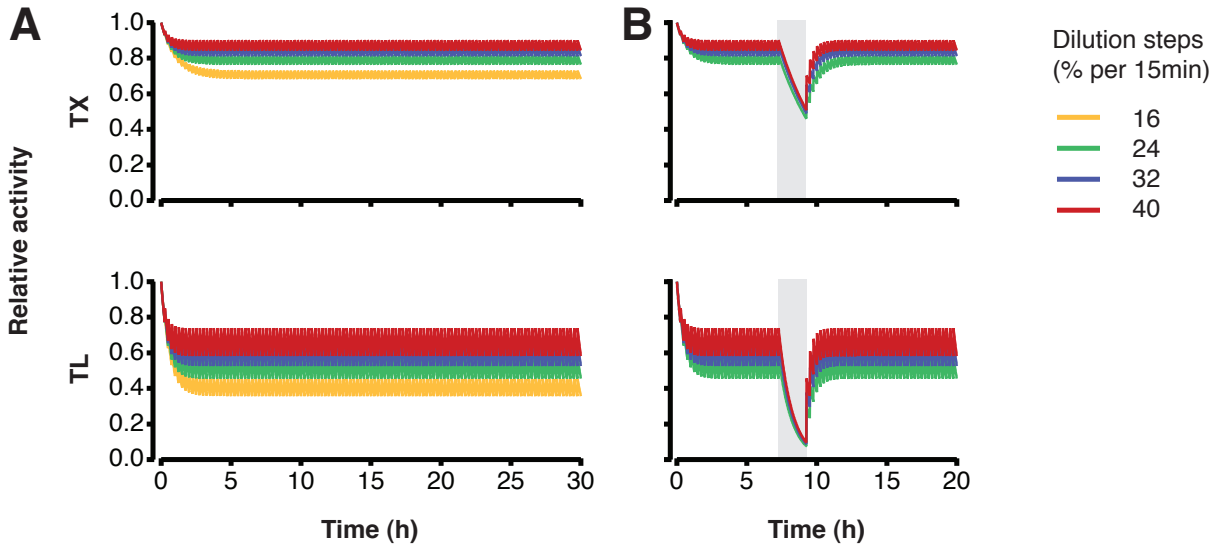

Fig. S18. Predicted relative transcriptional and translational activities at different reaction conditions. (**A**) Long-term steady state ITT at different dilution rates. The predicted relative transcriptional and translational activities shown here correspond to the experiment and predictions in figure 2B. (**B**) Transient switch to batch conditions. No dilutions occurred in the shaded time span. The predicted relative transcriptional and translational activities shown here correspond to the experiment and predictions in figure 2C. Relative activities were modeled with discrete dilution steps every 15min, which cause the teeth-like fluctuations.

Model of the repressilator in batch and continuous reaction

The repressilator consists of three transcriptional repressors, which each inhibit the expression of the preceding gene in the network (7). We modeled the repressilator as a symmetric system, where all repressors are identical except for their DNA-binding specifities, using the following differential equations for mRNA and protein concentration of the three repressors, R1-3 (i = R2, R3, R1 and j = R1, R2, R3):

$$m_i'(t) = act_{TX}(t) \cdot \frac{TX \cdot Km^n}{Km^n + p_j^n} - \deg_m \cdot m_i(t) - dil \cdot m_i(t),$$

$$p_i'(t) = act_{TL}(t) \cdot \frac{m_i(t)}{m_{total}(t)} \cdot TL(m_{total}(t)) - \deg_p \cdot p_i(t) - dil \cdot p_i(t).$$

We set the transcription rate at the unrepressed state, TX, of each promoter to 3nM/min, the Michaelis constant, Km, to 40nM and the Hill coefficient, n, to 2. The translation rate, TL, was calculated from equation 18. To take into account saturation of the translation machinery at high mRNA concentration we determined the translation rate for total mRNA concentration, m_{total}, and scaled by the fraction of mRNA concentration of the repressor modeled in that case.

Transcription and translation activities were modeled as above, using the following differential equations:

$$act_{TX}'(t) = -\deg_{TX} \cdot act_{TX}(t) - dil \cdot act_{TX}(t) + dil,$$

$$act_{TL}'(t) = -\deg_{TL} \cdot act_{TL}(t) - dil \cdot act_{TL}(t) + dil.$$

We compared behavior of the oscillator under batch and continuous reaction conditions. Additionally we modeled an "improved" batch reaction, where mRNA degradation and protein degradation rates are increased to *in vivo* levels of *E. coli* (8, 9), and where the rates of activity decrease of transcription and translation were a 10^{th} of the rates we measured. These improvements seem experimentally feasible, if mRNA and protein degradation mechanisms (8) and feeding of the ITT reaction by diffusion of small molecules (10, 11) were combined. The values of the following parameters were varied as follows in the three different reaction conditions:

	Reaction conditions		
Parameter	**Batch**	**Improved batch**	**Continuous**
Dilution rate, *dil*	0	0	$1.54h^{-1}$
mRNA degradation, deg_m	$0.003min^{-1}$	$0.053min^{-1}$	$0.003min^{-1}$
Protein degradation, deg_p	0	$0.017min^{-1}$	0
Decrease of transcriptional activity, deg_{TX}	$0.005min^{-1}$	$0.0005min^{-1}$	$0.005min^{-1}$
Decrease of translational activity, deg_{TL}	$0.017min^{-1}$	$0.0017min^{-1}$	$0.017min^{-1}$

Initial conditions were 1nM for all mRNA species, 0 for protein concentrations of R1 and R2 and 100nM of protein R3. Initial relative transcriptional and translational activities were 1. We show concentration of repressor protein R3 in Fig. 1E.

Model of the genetic oscillator built in this study

We modeled the genetic oscillator (see Fig. 4 for a diagram) with a set of 13 differential equations. We assume that general parameters of the ITT reaction are the same as determined for EGFP synthesis. Specifically, we use the same degradation rate, deg_m, for all RNA species as measured for EGFP mRNA, and the same translation rate TL. Also, decrease of transcriptional and translational activities were modeled as above, with the following two differential equations:

$$act_{TX}'(t) = -\deg_{TX} \cdot act_{TX}(t) - dil \cdot act_{TX}(t) + dil ,$$

$$act_{TL}'(t) = -\deg_{TL} \cdot act_{TL}(t) - dil \cdot act_{TL}(t) + dil .$$

RNA (m) synthesis from the TetR repressed T3tet promoter controlling the genes for T3RNAP and Cerulean were modeled by the following differential equations:

$$m_{\text{T3RNAP}}'(t) = act_{TX}(t) \cdot \frac{TX_{\text{T3RNAP}}(p_{\text{T3RNAP}}) \cdot K_{TetR}{}^{n}}{K_{TetR}{}^{n} + p_{TetR}{}^{n}} - \deg_m \cdot m_{\text{T3RNAP}}(t) - dil \cdot m_{\text{T3RNAP}}(t) ,$$

$$m_{\text{Cerulean}}'(t) = act_{TX}(t) \cdot \frac{TX_{\text{Cerulean}}(p_{\text{T3RNAP}}) \cdot K_{TetR}{}^{n}}{K_{TetR}{}^{n} + p_{TetR}{}^{n}} - \deg_m \cdot m_{\text{Cerulean}}(t) - dil \cdot m_{\text{Cerulean}}(t) ,$$

and RNA concentrations synthesized from unrepressed T3 promoter (*supD*, *tetR*, Citrine genes) were modeled with the following differential equations:

$$m_{\text{supD}}'(t) = act_{TX}(t) \cdot TX_{\text{supD}}(p_{\text{T3RNAP}}) - \deg_m \cdot m_{\text{supD}}(t) - dil \cdot m_{\text{supD}}(t) ,$$

$$m_{\text{tetR}}'(t) = act_{TX}(t) \cdot TX_{\text{tetR}}(p_{\text{T3RNAP}}) - \deg_m \cdot m_{\text{tetR}}(t) - dil \cdot m_{\text{tetR}}(t) \text{ and}$$

$$m_{\text{Citrine}}'(t) = act_{TX}(t) \cdot TX_{\text{Citrine}}(p_{\text{T3RNAP}}) - \deg_m \cdot m_{\text{Citrine}}(t) - dil \cdot m_{\text{Citrine}}(t) .$$

In all these RNA synthesis equations, transcriptional activation of the different genes by different concentrations of T3RNAP was described with:

$$TX_{gene}(p_{\text{T3RNAP}}) = \frac{TX\max_{gene} \cdot p_{\text{T3RNAP}}{}^{m}}{K_{\text{T3RNAP}}{}^{m} + p_{\text{T3RNAP}}{}^{m}} .$$

Changes in protein concentration, p, for T3RNAP, Citrine and Cerulean were modeled with the following differential equations. Like EGFP, Citrine and Cerulean have a dark and a fluorescent state, and we assume the same maturation rate (mat), as determined for EGFP:

$$p_{\text{T3RNAP}}'(t) = act_{TL}(t) \cdot \frac{m_{\text{T3RNAP}}(t)}{m_{total}(t)} \cdot TL(m_{total}(t)) - dil \cdot p_{\text{T3RNAP}}(t) ,$$

$$p_{\text{Cerulean}_d}'(t) = act_{TL}(t) \cdot \frac{m_{\text{Cerulean}}(t)}{m_{total}(t)} \cdot TL(m_{total}(t)) - mat \cdot p_{\text{Cerulean}_d}(t) - dil \cdot p_{\text{Cerulean}_d}(t),$$

$$p_{\text{Cerulean}_f}'(t) = mat \cdot p_{\text{Cerulean}_d}(t) - dil \cdot p_{\text{Cerulean}_f}(t),$$

$$p_{\text{Citrine}_d}'(t) = act_{TL}(t) \cdot \frac{m_{\text{Citrine}}(t)}{m_{total}(t)} \cdot TL(m_{total}(t)) - mat \cdot p_{\text{Citrine}_d}(t) - dil \cdot p_{\text{Citrine}_d}(t),$$

$$p_{\text{Citrine}_f}'(t) = mat \cdot p_{\text{Citrine}_d}(t) - dil \cdot p_{\text{Citrine}_f}(t).$$

For synthesis of TetR protein, stop codon suppression mediated by *supD* RNA had to be taken into account:

$$p_{tetR}'(t) = act_{TL}(t) \cdot \frac{m_{tetR}(t)}{m_{total}(t)} \cdot TL(m_{total}(t)) \cdot \frac{RT_{\max} \cdot m_{\sup D}(t)}{K_{\sup D} + m_{\sup D}(t)} - dil \cdot p_{tetR}(t).$$

Translation of each individual mRNA species was scaled to total (translated) mRNA, $m_{total} = m_{T3RNAP} + m_{tetR} + m_{Cerulean} + m_{Citrine}$.

We only have rough estimates of the individual parameters for transcription and translation of the different genes in the network as a function of their regulator concentrations. In the table below we list the values of the parameters that we used in the model to compare our experimental results (see below) and a reasonable range in which we think this value could differ (these estimates are based the results in Fig. 3, on our experience and initial experiments in batch format):

Parameter	**Value used in model**	**Probable range**
maximal transcription rates, $TXmax_{r,u}$ (at saturation T3RNAP concentration and unrepressed, and for the DNA template concentrations used in this study):		
$TXmax_{T3RNAP}$	7.5 nM/min	1 – 30 nM/min
$TXmax_{supD}$	20 nM/min	1 – 40 nM/min
$TXmax_{tetR}$	10 nM/min	1 – 30 nM/min
$TXmax_{Citrine,Cerulean}$	1 nM/min	0.2 – 10 nM/min
Michaelis-Menten constants (affinities) of TetR, T3RNAP and supD amber suppressor tRNA to their target sites:		
K_{tetR}	40 nM	20 – 500 nM
K_{T3RNAP}	500 nM	20 – 500 nM
K_{supD}	1000 nM	100 – 10 000 nM
Hill coefficients of TetR, T3RNAP and *supD* amber suppressor tRNA binding:		
for TetR: n	2	1 – 2
for T3RNAP: m	2	1 – 3
for *supD* (not modeled)	1	1 – 2
Maximal readthrough, stop codon suppression by supD amber suppressor tRNA (ratio of translated to untranslated mRNA):		
RT_{max}	0.5	0.001 – 0.9

Initial conditions were 25nM of T3RNAP mRNA and a transcriptional and translational activity of 1. Note that in our experiments it was not necessary to use an initial concentration of T3RNAP protein or mRNA, which was due to transcriptional leakage (leakage was not modeled here). Many parameter combinations in the probable range produced oscillations for broad ranges of feasible dilution rates. Generally, it was beneficial to have a low K_{tetR} value and medium to high transcription rates. The combination of parameters listed in the table above produced results that were very similar to our experimental observations but generally the oscillations had a longer period and occurred at slightly lower dilution rates than in the experiments. As in our experiments, we observed three different general behaviors as a function of dilution rate (Fig. S6). At low dilution rates we observed one peak of reporter proteins. At intermediate dilution rates we observed sustained or dampened oscillations, and at high dilution rates reporter protein concentrations stayed low. To reproduce the experiments shown in Fig. S3, we set the maximal transcription rates, TXmax, of one of the network components at a time to zero using a constant dilution rate that produced oscillations, when all network components were expressed. This resulted in the expected results that had also been observed in the experiment: no synthesis for $TXmax_{T3RNAP} = 0$; a stable steady state reporter synthesis for $TXmax_{supD} = 0$ and a slightly higher stable steady state reporter synthesis for $TXmax_{tetR} = 0$ (Fig. S7).

References:

1. Hansen CL, Sommer MOA, Quake SR (2004) Systematic investigation of protein phase behavior with a microfluidic formulator. *Proc Natl Acad Sci USA* 101:14431–14436.

2. Ridgeway WK, Seitaridou E, Phillips R, Williamson JR (2009) RNA-protein binding kinetics in an automated microfluidic reactor. *Nucleic Acids Res* 37:e142–e142.

3. Galas J-C, HAGHIRI-GOSNET A-M, Estévez-Torres A (2013) A nanoliter-scale open chemical reactor. *Lab Chip* 13:415–423.

4. Unger M, Chou H, Thorsen T, Scherer A, Quake S (2000) Monolithic microfabricated valves and pumps by multilayer soft lithography. *Science* 288:113.

5. Niederholtmeyer H, Xu L, Maerkl SJ (2012) Real-Time mRNA Measurement during an in Vitro Transcription and Translation Reaction Using Binary Probes. *ACS Synth Biol* 8:411-417.

6. Stögbauer T, Windhager L, Zimmer R, Rädler JO (2012) Experiment and mathematical modeling of gene expression dynamics in a cell-free system. *Integr Biol (Camb)* 4:494–501.

7. Elowitz MB, Leibler S (2000) A synthetic oscillatory network of transcriptional regulators. *Nature* 403:335–338.

8. Shin J, Noireaux V (2010) Study of messenger RNA inactivation and protein degradation in an Escherichia coli cell-free expression system. *J Biol Eng* 4:9.

9. Andersen JB et al. (1998) New unstable variants of green fluorescent protein for studies of transient gene expression in bacteria. *Appl Environ Microbiol* 64:2240–2246.

10. Noireaux V, Libchaber A (2004) A vesicle bioreactor as a step toward an artificial cell assembly. *Proc Natl Acad Sci USA* 101:17669–17674.

11. Shin J, Noireaux V (2012) An E. coli cell-free expression toolbox: application to synthetic gene circuits and artificial cells. *ACS Synth Biol* 1:29–41.